

ANALYSIS OF TONAL NOISE OF LPT BASED ON UNSTEADY GAS FLOW CALCULATIONS

R.Z. Nigmatullin*, L.V. Terentyeva*
CIAM*, Moscow

Keywords: *tonal noise, low pressure turbine, unsteady calculations*

Abstract

A study of tonal noise generated by the two-stage low-pressure turbine was performed for different operating modes. The analysis is based on numerical integration of Reynolds averaged three-dimensional unsteady Navier-Stokes equations (URANS) describing turbulent flows of viscous heat-conducting gas. The calculated pressure field is converted by methods of spectral, radial and modal analysis to get the tonal characteristics of the noise generated in the turbine exit. The results are compared with available experimental data and the results of numerical integration of linearized Euler equations. Other examples of tonal noise calculation are presented as well.

1 Introduction

In recent years aircraft engine noise has been significantly reduced. This was mainly achieved by reducing noise of fan and jet which are the main sources of the engine noise. Increasing bypass ratio in modern engines also tends to reduce jet and fan noise. Against these successes low-pressure turbine noise has become more important. In particular, at approach regime turbine may become the dominant source of noise in the certain frequency range, while the other engine components noise is quite low. Currently LPT noise is not well studied, because it has been considered earlier as less important. There is practically no way to predict LPT noise especially for the new types of turbines. Application of cut off rule at the design not always leads to the turbine noise reduction. In addition, there is almost no possibility to reduce

the LPT noise using acoustic lining, as there is no available light-weight and high-temperature resistant materials [1].

Within the framework of the European research project VITAL test rigs for research of LPT acoustic characteristics were created to verify analytical and numerical methods used in turbomachinery for noise estimation. The experiments allow to verify numerical methods and to clarify sound generation mechanisms in the turbine [2]. Data of similar tests carried out at a European research center were used in the present paper.

Numerical evaluation of the turbine tonal noise can be performed using either semi-empirical approaches and approaches based on the solution of the linearized equations for the perturbations or methods where the initial nonlinear governing equations are solved [3]. Latter approach requires significantly higher computational costs because of the necessity of very fine computational grids use. Corresponding numerical investigation has been carried out to estimate perspective of similar methods.

2 Numerical method

2.1 CFD simulation

The calculations were performed based on the Reynolds averaged 3D unsteady Navier-Stokes equations that describe the turbulent flow of viscous heat-conducting gas. The equations are written in cylindrical coordinates in conservative form. The computational domain for the unsteady calculation contains several blade and vane channels for each stage.

Numerical grids for nearby stages join along the surface, located approximately in the middle of the axial gap between them. It is assumed that the radial clearance is zero but tip surfaces of shrouded blades rotate. Turbulence effects were modeled using the one-parameter differential turbulence model of Spalart and Allmaras [4]. Numerical solution of unsteady equations of gas motion has been found using the implicit high order accuracy numerical scheme [5]. The scheme has second (for model conditions even fifth) order of approximation in space and the second order in time. In unsteady calculations at the slipping interface between neighboring grids a conservative procedure was used. Solid walls (blade and vane surfaces, hub and tip limiting surfaces) were supposed adiabatic. At the inlet section all parameters were assumed constant along the radial and circumferential directions.

In unsteady flow calculations non-reflecting boundary conditions were specified at the outlet section. Data required for these conditions were taken from the results of the corresponding steady calculations.

2.2 Radial functions calculation

Static pressure distribution $p(t, r, \theta)$ in an axial section at the turbine exit, obtained in the unsteady calculation, is then investigated by use of frequency-modal and radial analysis, based on the following decomposition:

$$p(t, x, r, \theta) = \sum_{k, m, n}^{+\infty} \left(A_{mn} e^{ik_{mn}x} \right) f_{mn}(r) e^{i(m\theta - \omega_k t)} \quad (1)$$

where ω_k – the frequency of oscillations, associated with the rotational speed of the turbine and the first and second stage blade numbers by relation $\omega_k = \Omega(j_{1k} B_1 + j_{2k} B_2)$; m and n – circumferential and radial order of the mode respectively; k_{mn} – wave number, A_{mn} – the complex amplitude of the mode (m, n) ; $f_{mn}(r)$ – eigenfunction describing acoustic swirling flow in a duct.

It is known that in the case of uniform axial mean flow a propagation of acoustic perturbations in a circular channel duct can be described analytically using the Bessel functions of the first and second kind. In the general case of swirling mean flow with axial shift acoustic

and vortex disturbances, propagating in the duct, interact, and the analytical solution does not exist. In this case, the eigenvalues and eigenfunctions can be found numerically. In the present work radial eigenfunctions were found numerically using the spectral method, described in detail in [6].

3 Results for a two-stage LPT

A model two-stage uncooled low pressure turbine is considered. The results of all unsteady calculations were being saved at each time step in three axial sections: the first of them is at the middle of axial gap between the second vane row and second blade row, the second section is located close to the second blade trailing edges and the third one is close to the exit section. Grids for the stages join along the surface, located approximately in the middle of the axial gap between them.

The calculations were performed using H-type numerical grids. To get more uniform grids across the viscous shear flow around solid surfaces (at limited computer resources) wall functions in the version of Reichardt [7] were used in the calculations. Non-dimensional thickness of the cells adjacent to solid walls has averaged value $y^+ \sim 50$. Within the computational domain for one blade or vane channel typically 30 cells were used in the circumferential and radial directions, in the stream wise direction the number of cells was 60 to 120.

The calculation of the low-pressure turbine noise was performed for a number of different regimes.

Flow field in the turbine axial gaps contains significant fluctuations of velocity, pressure, temperature. These fluctuations generate tonal noise when interacting with the blades and vanes. Figure 1 shows an instant pattern of the isentropic Mach number – pressure function – distribution (bandage shrouds above the blades are not shown).

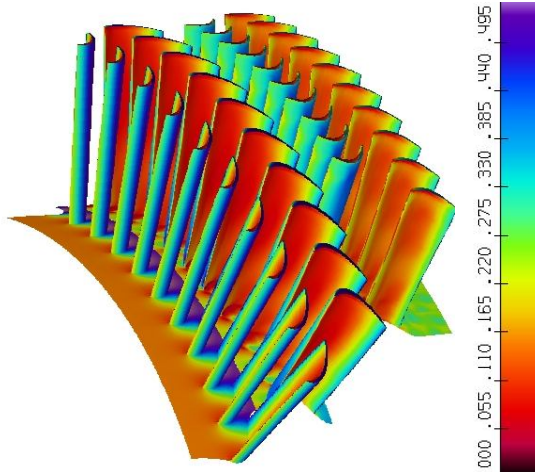


Fig. 1. Instant pattern of the isentropic Mach number distribution.

Figure 2 shows a typical graph of pressure pulsations (along time steps) in a point in the middle of the second blade channel at the mean radius.

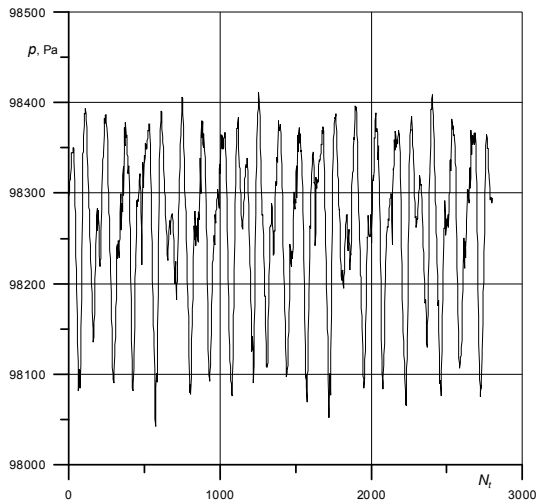


Fig. 2. Static pressure distribution at the mean radius in the middle of the second blade channel.

Calculation of frequency-modal spectrum of pressure pulsations in the section at the turbine exit is based on the relation (1). Dependence of the amplitude A_{mn} for each frequency-modal harmonic on the radial coordinate r expands in series of basic functions $f_{mn}(r)$, corresponding to acoustic eigen-solutions of the swirling flow. The parameters of mean stationary flow, used for eigenfunctions calculation, are determined by the radial distributions of the Mach number and sound speed.

Figure 3 shows eigenfunctions $f_{mn}(r)$ for the propagating radial modes for the regime

Approach. The first number in the line notation corresponds to the frequency (in Fig. 3-5 we use notation $g=\omega_k/\Omega$); the second number corresponds to order of the circumferential mode m ; radial order n is determined by the number of zeros of the function.

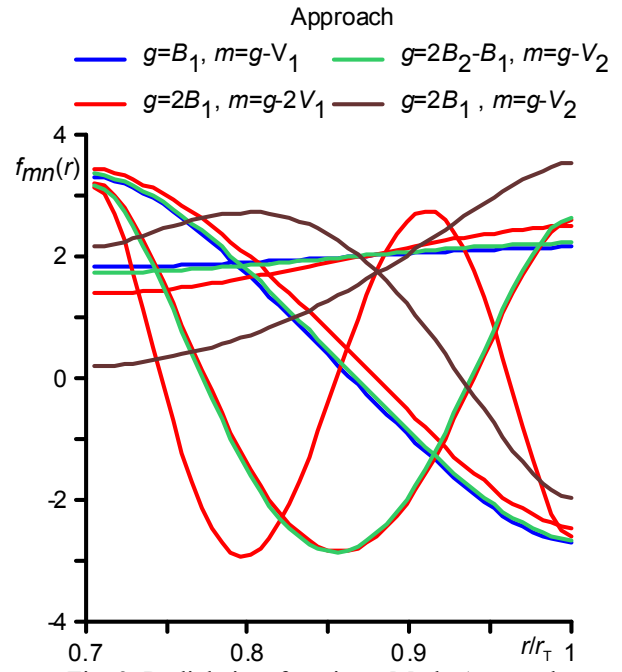


Fig. 3. Radial eigenfunctions. Mode Approach.

In order to estimate the influence of grid density in the radial direction on the accuracy of the tonal noise prediction additional calculations were fulfilled. The calculations were once performed using a coarse grid with the number of cells in a radial direction 20, and other time using finer grid with the number of cells in a radial direction 40.

In Fig. 4-5 graphs of the radial distributions of amplitude of one of spectral-modal components of pressure pulsations for some values of frequencies ω_k and circumferential mode m for Approach and Cut back regimes are shown. Additionally the results of linearized Euler equations approach [8] are plotted (3DAS).

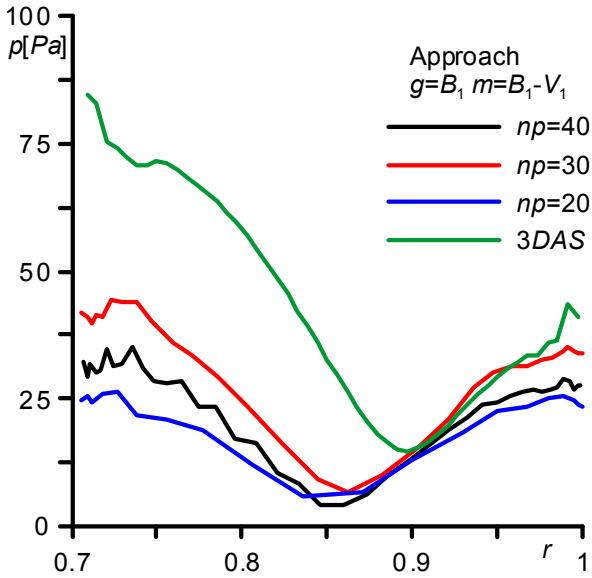


Fig. 4. Radial distributions of amplitude of pressure pulsation component for Approach regime for frequency $\omega_k=B_1\Omega$ and circumferential mode $m=B_1-V_1$.

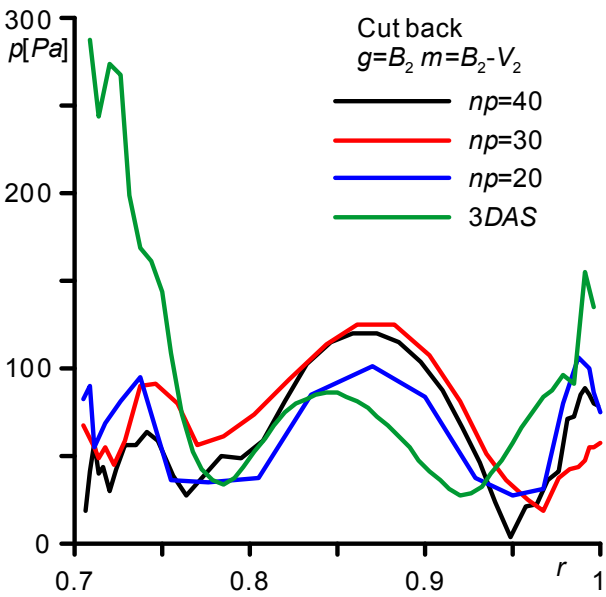


Fig. 5. Radial distributions of amplitude (in Pa) of pressure pulsation component for Cut back regime for frequency $\omega_k=B_2\Omega$ and circumferential mode $m=B_2-V_2$.

In general, the results of computations on different grids are close to each other but differ from the results of the linearized model.

Figures 6-7 show amplitudes of various components of the frequency-modal and radial spectrum (not all of the propagating modes are shown). The pictures show the results of acoustic tests, URANS calculations (for different grids) and the results of calculations based on the linearized Euler equations (3DAS).

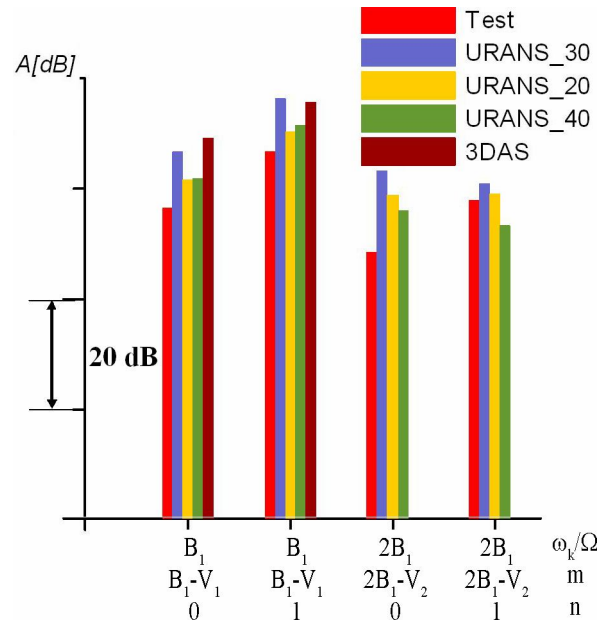


Fig. 6. Amplitudes of some components of the frequency-modal and radial spectrum. Approach regime.

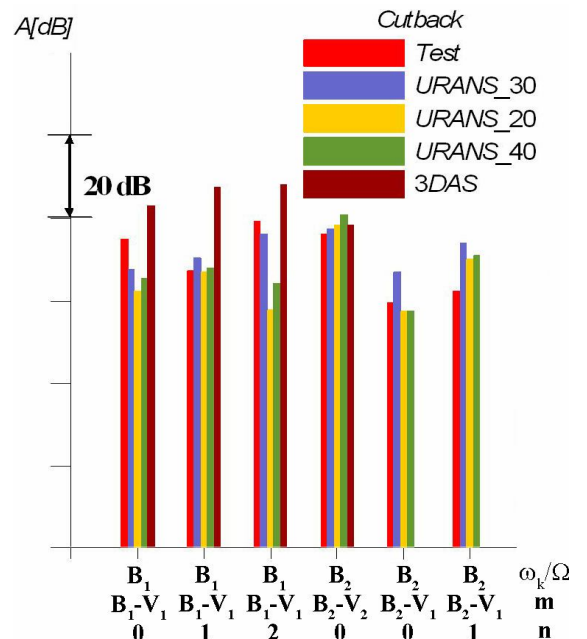


Fig. 7. Amplitudes of some components of the frequency-modal and radial spectrum. Cut back regime.

The comparison between obtained results of tonal noise turbine simulation and acoustic measurements shows that in general a difference of calculated results from the experiment does not exceed 10 dB at the lower frequencies but increases with the frequency of pressure pulsations component. The best results are achieved for the main blade passing frequency of the second rotor.

4 Investigation of clocking effect

Unsteady aerodynamic calculation of the multistage low-pressure turbine of an aircraft engine was performed.

Numbers of rotor blades in two considered neighboring stages are equal ($V_1=V_2$ и $B_1=B_2$), so an attempt was made to improve the flow pattern by the circumferential vane and blade shifts in the second stage. Separate calculations were performed for the considered two stages of LPT with different mutual circumferential shifts of the second vane row and second blade row. The vane row of the second stage was turned (as a whole) around the turbine axis by a certain angle so that (time averaged) wakes from the vanes of the first stage exactly impinges on the leading edges of the second stage vanes (the turn angles were found based on the unsteady calculation results for the initial geometry). Similar modification has been applied to the second blade row. For the obtained optimal position the unsteady calculation was performed. Distributions of “total pressure loss” coefficient $\xi=(p_1^*-p^*)/(p_1^*-p_2)$ at different radii of span for the second vane and blade are shown in Fig. 8. Here p_1^* is averaged total pressure at the vane (blade) row inlet section, p^* is current total pressure, p_2 is averaged static pressure at the vane (blade) row exit section.

As these figures show, the wakes from the upstream vanes (blades) impinge close to the leading edges of the considered vanes (blades) at the mean radius. However at the hub area the wakes from the first stage vanes pass the second stage vane-to-vane channel between the vanes. At the tip area the wakes pass the channel close to the suction sides of the vanes. Thus, the geometry of the second vane has the property that the wakes from the first vanes pass the vane-to-vane channel of the second stage in optimal way only at mean sections and it reduces the advantages of the clocking effect. The same is valid for rotor blades: the wakes from the first blades pass the blade-to-blade channel in optimal way at mean radius but they pass the channel at the tip area in most unfavorable way: in the middle between the blades.

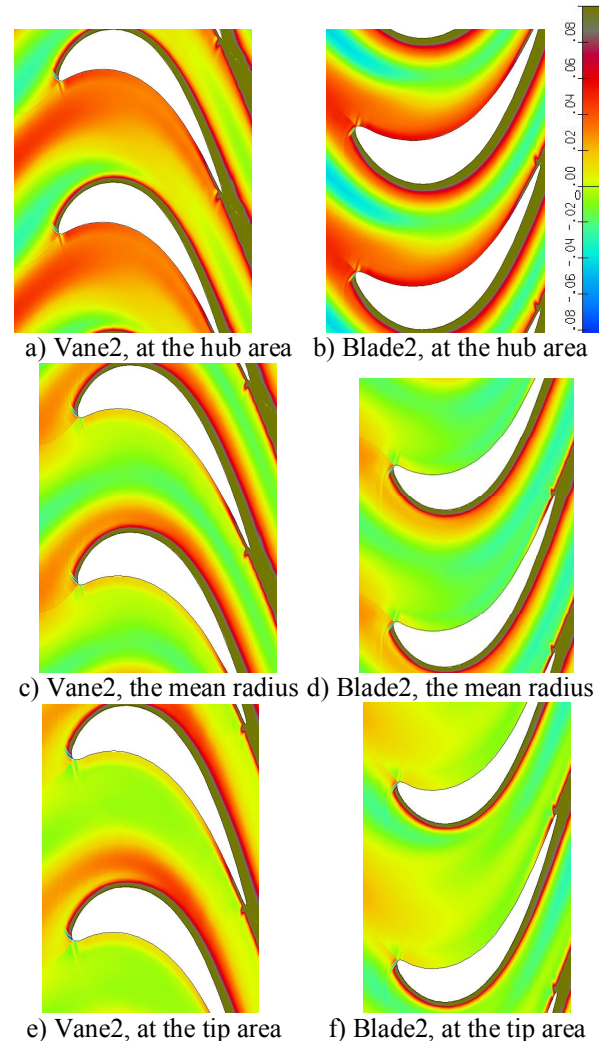


Fig. 8. Coefficient ξ distributions in different sections of the second stage. Separate calculation for a group of two neighboring stages of the LPT. Time averaged fields of the unsteady solution.

Three additional calculation runs were performed for the comparison. In the first calculation run the vanes and blades of the second stage were turned from the optimal position by quarter of the pitch in the direction from the pressure side to the suction side of the profile (i.e. in the direction of rotation for the blade and in opposite direction for the vane), in the second calculation run the vanes and the blades were turned by the half of the pitch, and in the third calculation run – by three-quarters of the pitch. Corresponding distributions of the coefficient ξ are shown in the Fig. 9.

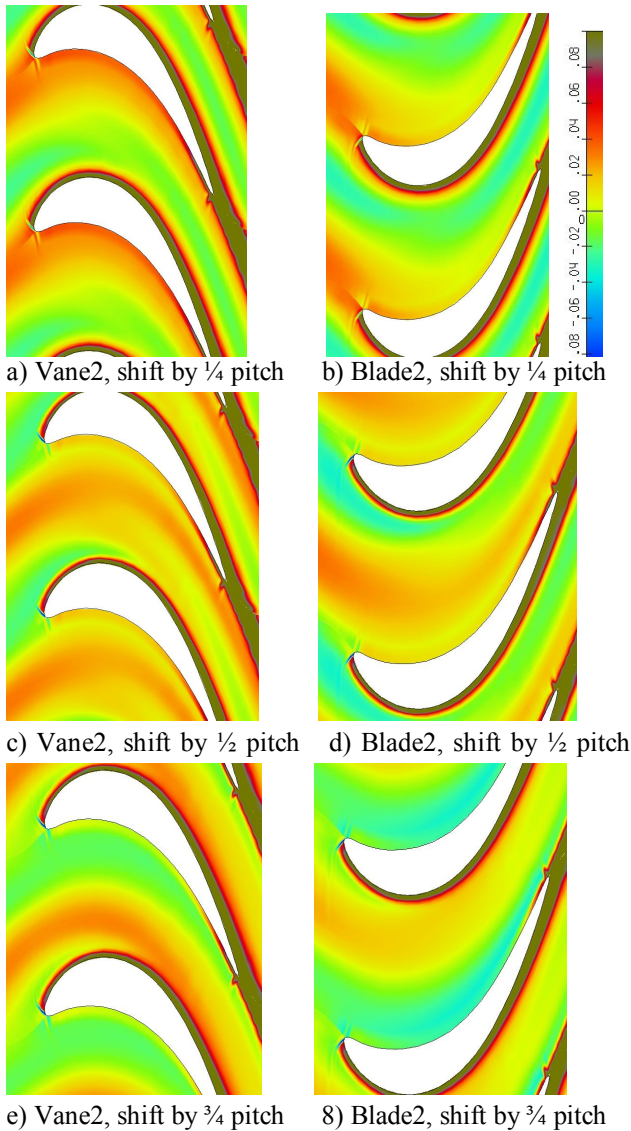


Fig. 9. Coefficient ξ distributions at the mean radius of the second stage. Separate calculation for a group of two neighboring stages of the LPT. Time averaged fields. Geometry variants with different shift of the 2d stage rows in the circumferential direction.

Calculated efficiency values for different configurations are: for favorable positions (var0) is 0.9099, for $\frac{1}{4}$ pitch shift (var1) is 0.9099, for $\frac{1}{2}$ shift (var2) is 0.9093, for $\frac{3}{4}$ pitch shift (var3) is 0.9090. The positions of the second stage vanes and blades, when the wakes from the first stage vanes and blades impinge on the leading edges (at the mean radius), lead to higher efficiency. But the resulting gain from the clocking effect is very small (and less than the accuracy of the calculations). The gain was achieved mainly in the vane row where wakes from the previous vanes pass the passages in favorable way in upper part of the vanes.

However, in the lower part of the vanes the behavior of these wakes is unfavorable which reduces the effect. Similarly, in the second blade row the positive effect is small because the wakes passing picture in different sections of the blade row is different.

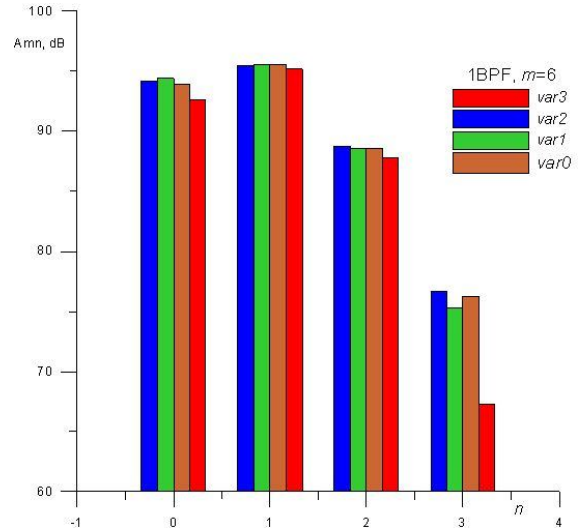


Fig. 10. Amplitude of mode (1bpf, 6) for different variants of circumferential shift of vane row.

On the basis of this study an attempt was made to evaluate the impact of the circumferential shift on the acoustic characteristics of the stages. The calculations were carried out for all four variants of the circumferential shift. Figure 10 presents the amplitude of the circumferential mode with the number $m=6=B_2-V_2=B_1-V_1$ and main blade passing frequency and different radial order n . The difference of the amplitudes did not exceed 1 dB and this is within the accuracy of the calculations. Thus, the influence of the circumferential shift of the second vanes and blades on the acoustic modes amplitudes in the calculations appears to be insignificant.

5 Last stage of a low pressure turbine

A last stage of a 5-stage low pressure turbine of an aviation engine is considered. The stage had initially 138 vanes and 121 blades. Calculated mode amplitudes are given in the table below.

Table. Mode amplitudes.

ω_k/Ω	m	n	A_{mn} , dB
121	17	0	99,2
		1	93,7
		2	87,6
		3	69,8

In accordance with cut off rule (for the Approach regime) it was proposed to increase the number of vanes up to 165. In this case at the main blade passing frequency all circumferential modes are not propagating, thus the effect of the turbine noise reducing is expected. But the modes connected with the interactions with the previous stages remain.

6 Conclusion

Low pressure turbine tone noise estimation method based on the solution of unsteady RANS equations is considered. The method allows the use of existing turbine flow calculation methods for the direct simulation of acoustic flows; however, it requires significantly finer grids and higher spatial accuracy, leading to increasing of required computations efforts. Relatively simple and quick processing of the unsteady calculations results by methods of Fourier analysis and radial eigenfunction decomposition allows to receive turbine tonal noise profile. Comparison of the obtained results with the available experimental data allows to judge about sufficient reliability of the method, but also requires additional investigations for high-frequency oscillations.

References

- [1] Nesbitt E. Towards a quieter low pressure turbine: design characteristics and prediction needs. *International Journal of Aeroacoustics*, Vol. 10, No. 1, pp 1-15, 2011
- [2] Broszat D, Korte D, Tapken U, Moser M, Validation of turbine noise prediction tools with acoustic rig measurements. *AIAA-2009-3283*, 2009.
- [3] Zante DV, Envia E. Simulation of turbine noise generation using a turbomachinery aerodynamics solver. *NASA/TM-2019-216230*, 1999.
- [4] Spalart PR, Allmaras SR. A One-Equation Turbulence Model for Aerodynamic Flows. *AIAA Paper- 92-0439*, 1992.
- [5] Ivanov M.Ja., Krupa V.G., Nigmatullin R.Z. Implicit high order Godunov's scheme for the integration of Navier-Stokes equations. *Journal of computational mathematics and mathematical physics*, 1989, vol. 29, pp. 888-901. (in Russian).
- [6] Kenneth A. Kousen. Eigenmodes of ducted flows with radially-dependent axial and swirl velocity component. *NASA/CR-1999-208881*, 1999.
- [7] Reichardt H. Die grundlagen des turbulent warmeuberganges. *Archives Gesamte Wärmetech*, pp 129-142, 1951.
- [8] Nyukhtikov M.A., Rossikhin A.A. Numerical method for calculating three-dimensional fan tonal noise due to rotor-stator interaction. *Proceedings of International Congress «Turbomachines: Aeroelasticity, Aeroacoustics, and Unsteady Aerodynamics»*, pp. 268-280. Moscow: TORUS PRESS Ltd., 2006.

Contact Author Email Address

mailto:nigma_rz@ciam.ru,
larisa@ciam.ru

Copyright Statement

The authors confirm that they, and/or their company or organization, hold copyright on all of the original material included in this paper. The authors also confirm that they have obtained permission, from the copyright holder of any third party material included in this paper, to publish it as part of their paper. The authors confirm that they give permission, or have obtained permission from the copyright holder of this paper, for the publication and distribution of this paper as part of the ICAS 2014 proceedings or as individual off-prints from the proceedings.